Universal folding pathways of polyhedron nets: Supplementary Information

Paul M. Dodd[a], **Pablo F. Damasceno**[b], **and Sharon C. Glotzer**[a,b,c,d]

[a]Chemical Engineering Department, University of Michigan, Ann Arbor, MI 48109, USA; [b]Applied Physics Program, University of Michigan, Ann Arbor, MI 48109, USA; [c]Department of Materials Science and Engineering, University of Michigan, Ann Arbor, MI 48109, USA; [d]Biointerfaces Institute, University of Michigan, Ann Arbor, MI 48109, USA

This manuscript was compiled on May 5, 2018

Image	Database Id	T_m	Diameter	Leaves	Paths
	0	2.50	3	2	2
	1	2.50	2	3	3
	0	4.10	4	3	9
	1	3.57	4	4	12
	2	3.10	4	3	6
	3	4.04	4	3	12
	4	4.16	5	2	6
	5	3.35	3	4	16
	6	4.15	5	2	2
	7	3.95	4	2	6
	8	3.99	5	4	8
	9	3.98	5	3	5
	10	3.74	3	4	18
	0	2.44	6	2	5
	1	2.49	6	3	7
	2	2.48	5	4	12
	3	2.56	7	3	6
	4	2.48	6	3	4
	5	2.49	7	2	6
	6	2.50	5	4	14
	7	2.45	5	3	12
	8	2.47	7	2	2
	9	2.50	5	3	12
	10	2.44	5	2	8

Table S1. Relevant data for the tetrahedron, cube, and octahedron nets. For each net, a database ID, melting temperature T_m, diameter, number of leaves, and number of paths connecting unfolded and folded states is shown.

a)

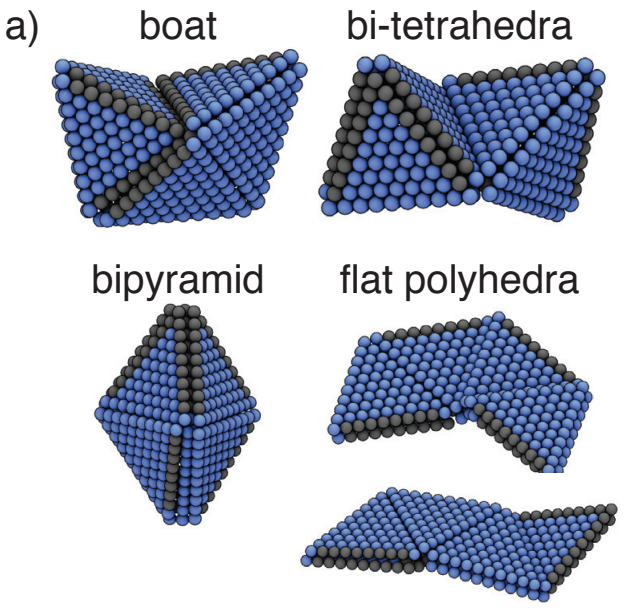

b)

Image	Database Id	Boat Prob. slow cooling (%)
	0	3.2
	1	0.0
	2	5.6
	3	0.0
	4	0.0
	5	0.0
	6	0.0
	7	12.7
	8	0.0
	9	2.4
	10	9.5

Fig. S1. Octahedron net misfolds. (a) Examples of trapped states that can be achieved by octahedron nets. The boat conformation occurs more often. (b) Probabilities of the octahedron nets folding into the boat conformation for the slow ($2.5\times10^{-8}T/t$) cooling rate.

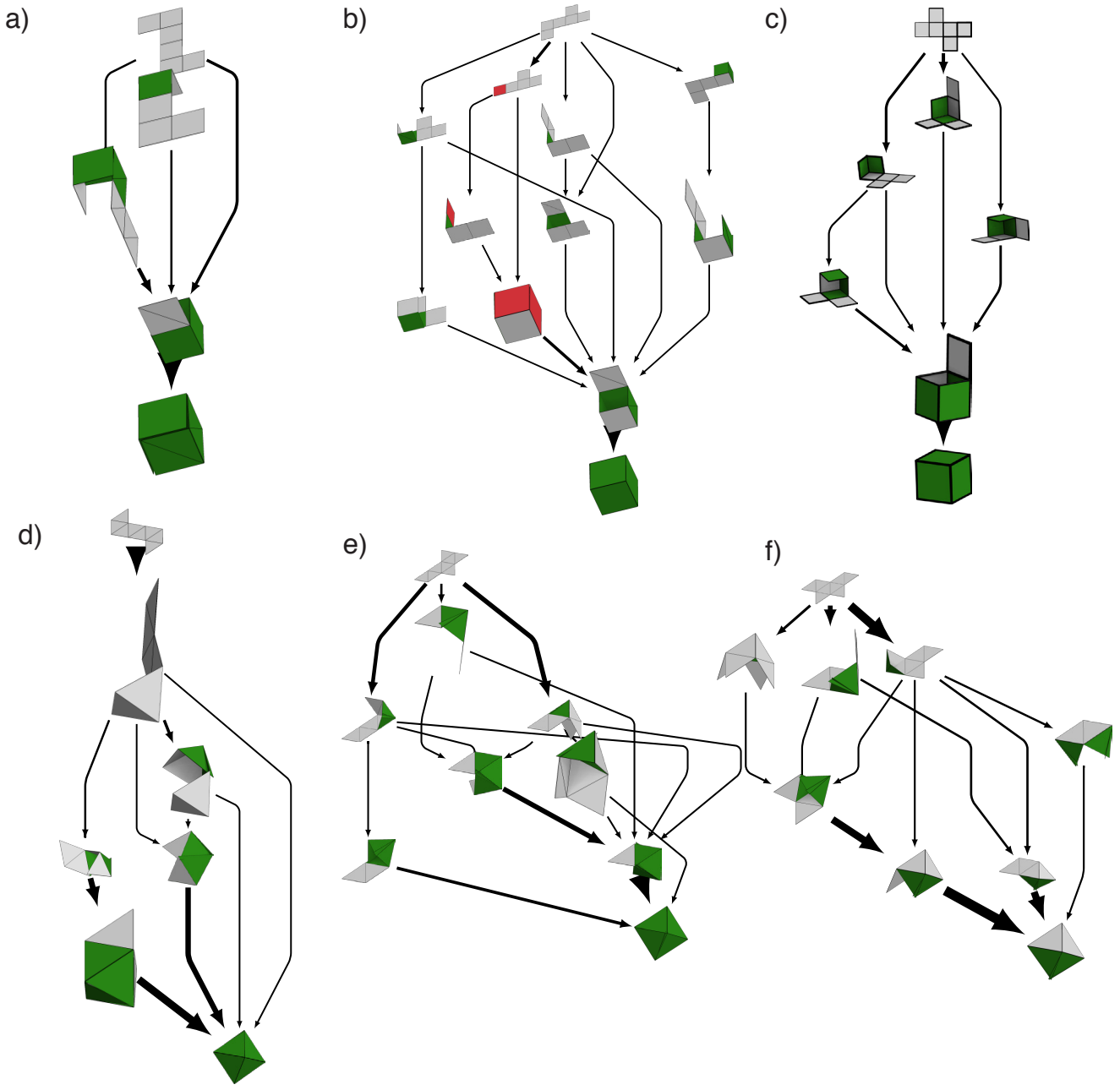

Fig. S2. Folding networks for representative cube and octahedron nets that have two (a,d), three (b,e), and four leaves (c,f). Networks were calculated at the melting temperature reported in Table S1.

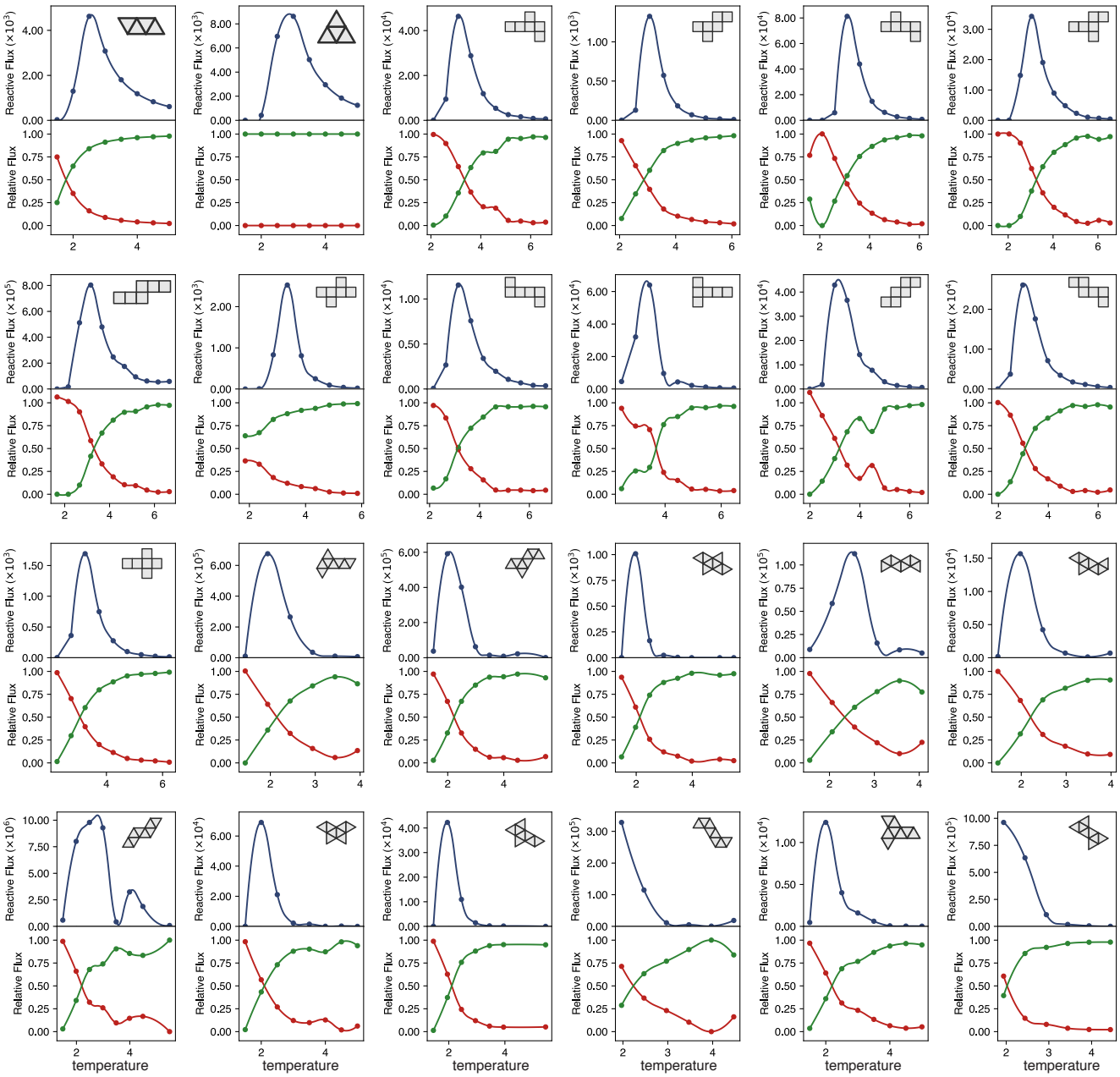

Fig. S3. Temperature dependence of reactive and relative fluxes for the tetrahedron, cube, and octahedron nets. The net corresponding to each plot is given as an inset. For each plot the blue curve represents the total reactive flux while the red and green curves represent the fraction of the flux corresponding to non-native and native contacts, respectively.

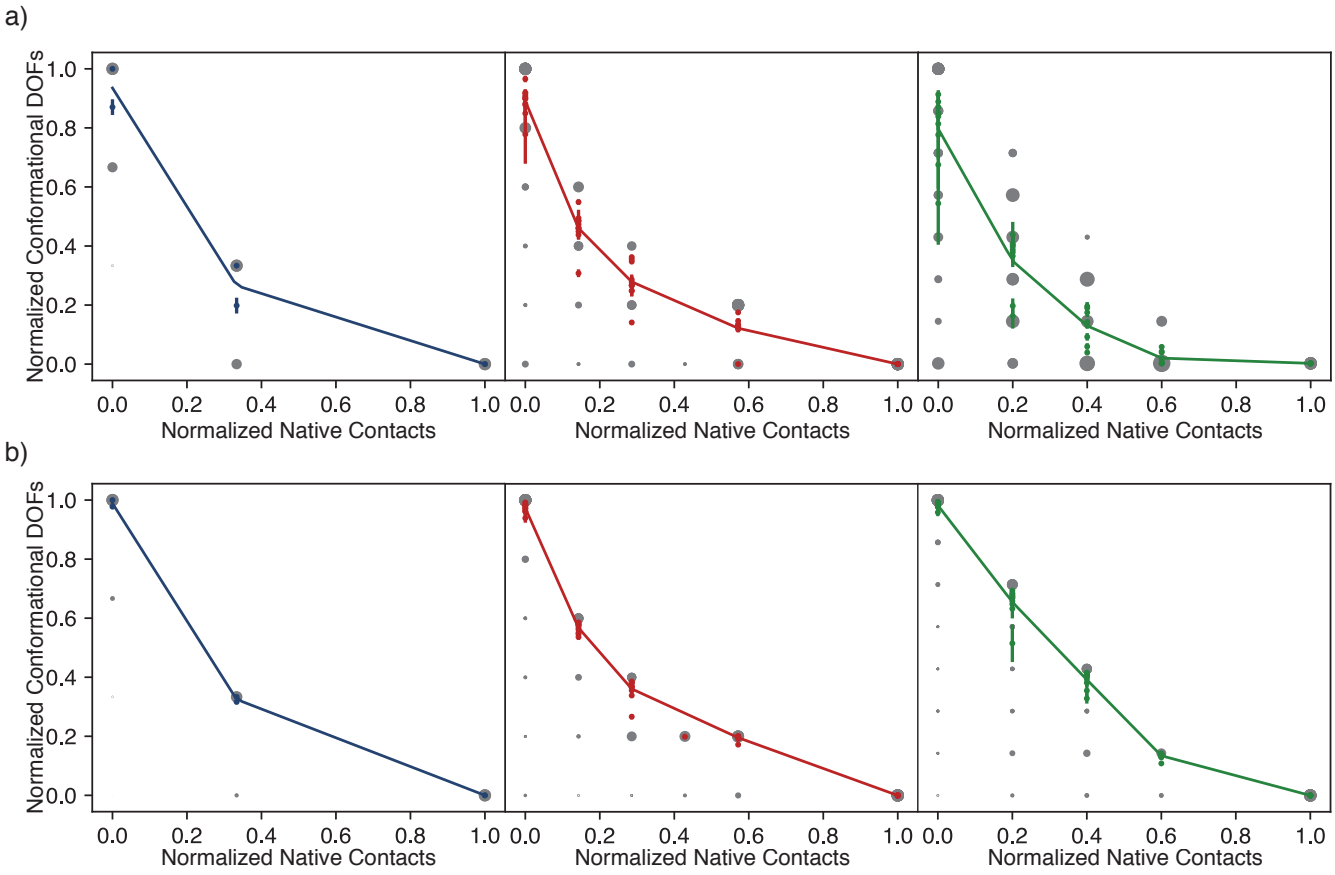

Fig. S4. The normalized conformational degrees of freedom of each net for the tetrahedron (blue), cube (red), and octahedron (green), as a function of the normalized number of native contacts for two different temperature regimes. All pathways from all net are projected onto this plot. Each gray point represents an intermediate observed in a reactive pathway and the size of each point is proportional to the probability that intermediate is in a reactive pathway. a) Pathways observed for a temperatures lower than the crossover temperature ($T = T_m - 1$). b) Pathways observed for a temperatures greater than the crossover temperature ($T = T_m + 0.5$). We find no correlation between the folding propensity and the proximity to the diagonal line at high temperature.

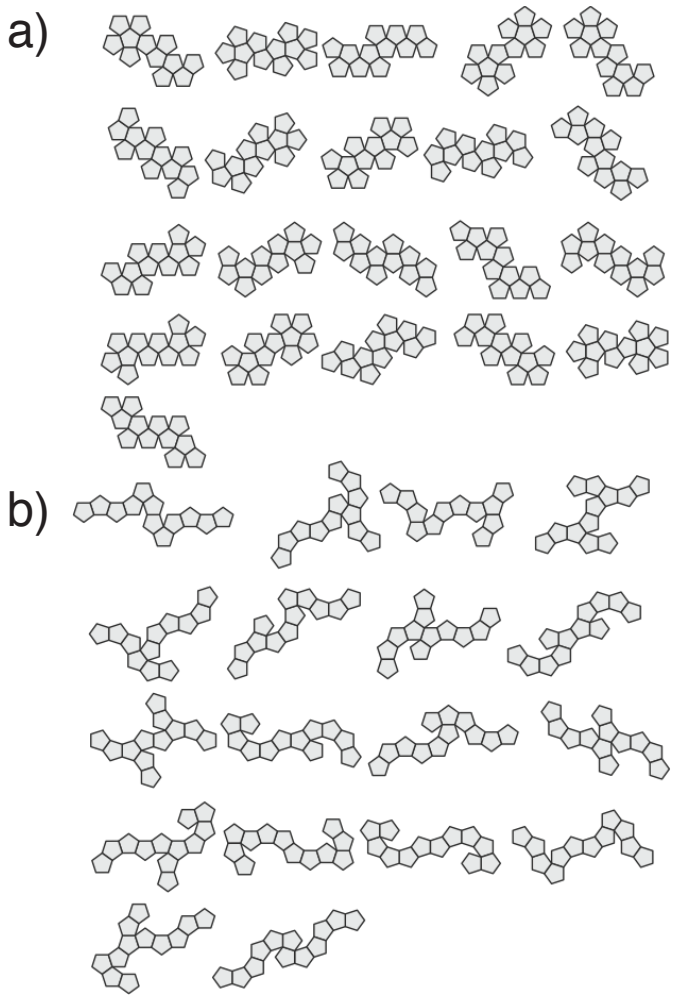

Fig. S5. Dodecahedron nets used in this study. Dodecahedron nets predicted to be “good” (a) folders and “bad” (b) folders.

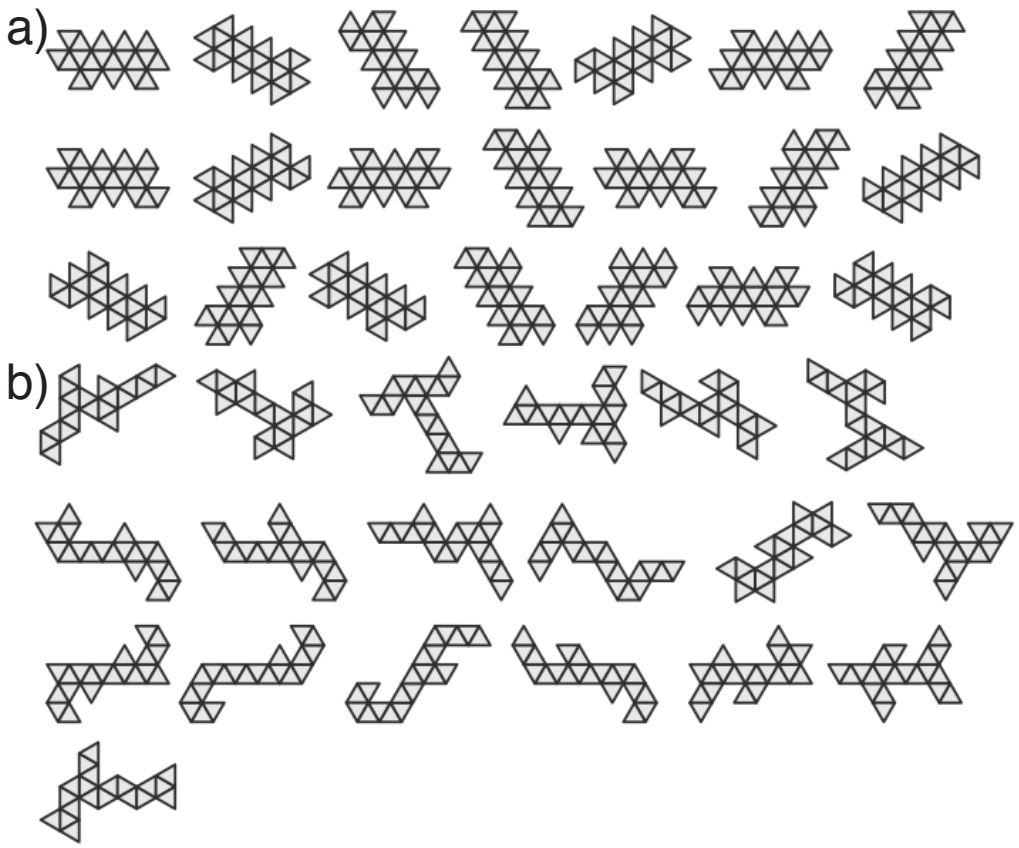

Fig. S6. Icosahedron nets used in this study. Icosahedron nets predicted to be “good” (a) folders and “bad” (b) folders.

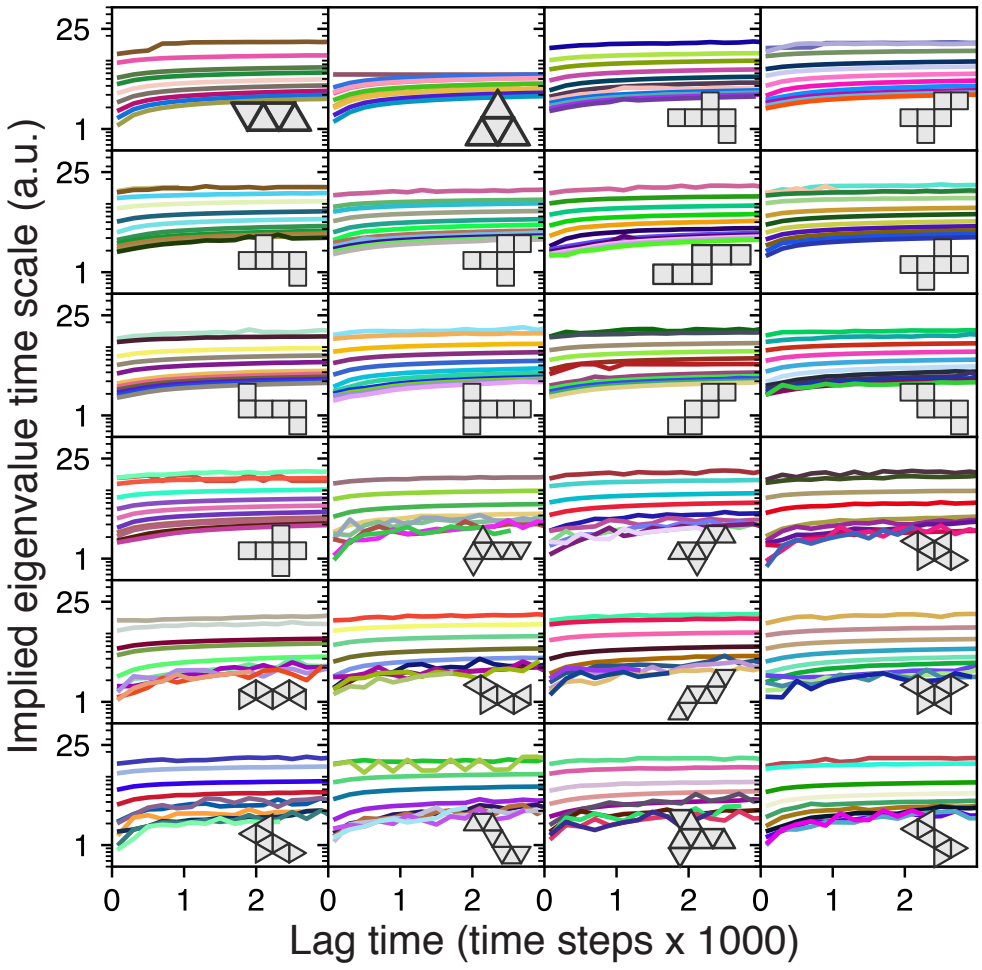

Fig. S7. Choice of lag time for MSM studies. For each tetrahedron, cube, and octahedron net (shown in the inset), the implied time scales is shown. Each curve shows the first non-trivial eigenvalue, λ_2, of the transition probability matrix, as a function of the lag time, τ, for a given temperature. The colors are random and distinguish different temperatures. All of the eigenvalues flatten out by $\tau = 1000$ time steps. We therefore choose this value as the lag time for each MSM study.